THE JOURNAL OF PHYSICAL CHEMISTRY B

Article

pubs.acs.org/JPCB

Molecular Modeling of Diffusion Coefficient and Ionic Conductivity of CO_2 in Aqueous Ionic Solutions

Miquel Garcia-Ratés,[†] Jean-Charles de Hemptinne,[‡] Josep Bonet Avalos,[†] and Carlos Nieto-Draghi*[,‡]

[†]Departament d'Enginyeria Química, ETSEQ, Universitat Rovira i Virgili, Avda. dels Països Catalans 26, 43007 Tarragona, Spain

[‡]IFP Energies nouvelles, 1 & 4 Av. De Bois-Préau, 92852 Rueil-Malmaison Cedex, France

Supporting Information

ABSTRACT: Mass diffusion coefficients of CO_2/brine mixtures under thermodynamic conditions of deep saline aquifers have been investigated by molecular simulation. The objective of this work is to provide estimates of the diffusion coefficient of CO_2 in salty water to compensate the lack of experimental data on this property. We analyzed the influence of temperature, CO_2 concentration,and salinity on the diffusion coefficient, the rotational diffusion, as well as the electrical conductivity. We observe an increase of the mass diffusion coefficient with the temperature, but no clear dependence is identified with the salinity or with the CO_2 mole fraction, if the system is overall dilute. In this case, we notice an important dispersion on the values of the diffusion coefficient which impairs any conclusive statement about the effect of the gas concentration on the mobility of CO_2 molecules. Rotational relaxation times for water and CO_2 increase by decreasing temperature or increasing the salt concentration. We propose a correlation for the self-diffusion coefficient of CO_2 in terms of the rotational relaxation time which can ultimately be used to estimate the mutual diffusion coefficient of CO_2 in brine. The electrical conductivity of the CO_2–brine mixtures was also calculated under different thermodynamic conditions. Electrical conductivity tends to increase with the temperature and salt concentration. However, we do not observe any influence of this property with the CO_2 concentration at the studied regimes. Our results give a first evaluation of the variation of the CO_2–brine mass diffusion coefficient, rotational relaxation times, and electrical conductivity under the thermodynamic conditions typically encountered in deep saline aquifers.

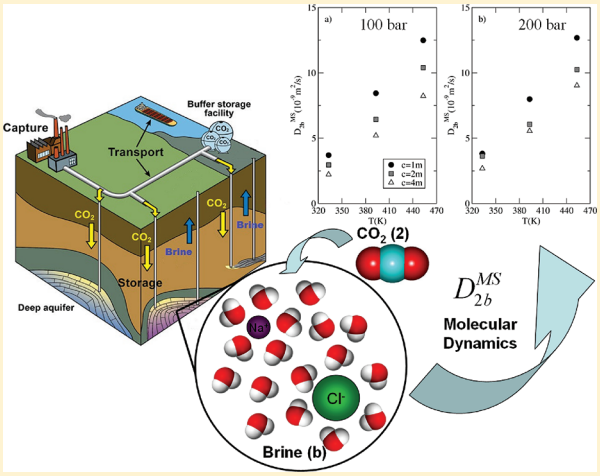

1. INTRODUCTION

The emission of greenhouse gases to the atmosphere due to strong industrial human activity is in general recognized to be the main cause of the increase of the global mean temperature on Earth in the 20th century.[1] After water vapor, CO_2 is the gas which contributes most to the greenhouse effect. The burning of fossil fuels like coal, oil, and natural gas as well as tropical lands deforestation have contributed to an accumulation of CO_2 in the atmosphere.[2] As a consequence, the atmospheric concentration of CO_2 has increased from 280 ppm in 1880 to 379 ppm in 2005.[1]

One of the important aspects related to CO_2 is the capacity of the natural reservoirs (biosphere and oceans) to reabsorb an important percentage of the CO_2 emitted to the atmosphere (approximately 30%).[1] However, while the residence time for the CO_2 in the biosphere is on the order of a decade, the residence time for the CO_2 in the deep oceans is on the order of a millenium. Therefore, among the economically and technically feasible options to reduce CO_2 emissions, the sequestration of CO_2 either in the deep ocean or in the geological media has become increasingly realistic. Candidate geological media include saline aquifers, oil/gas reservoirs, and coal formations.[3−5] Since the past decade, some CO_2 storage projects are in operation in different regions all over the world.[6−8]

Pressure and temperature in a geological formation depend on its depth. The mean temperature gradient in a geological formation varies between 25 and 30 °C/km, although in some cases it reaches 60 °C/km.[9] The surface temperature ranges between 5 and 20 °C, and the pressure ranges from 10 bar on the surface to 500 bar in the deepest aquifers.[9] Most of the proposed reservoirs to store the CO_2 are deeper than 500 m. By taking a look at the phase diagram of CO_2, we see that it becomes supercritical at $T > 31.1$ °C and $P > 73.8$ bar.[10] Hence, if we consider a mean temperature gradient of 30−60 °C/km, CO_2 will be supercritical at a depth close to 800 m. In terms of salinity, the main part of the geological formations has a high salinity, greater than 100 g/L, with typically chloride as the dominant anion and sodium as the dominant cation.[11,12] Only reservoirs with high salinity can be considered for CO_2 storage

Received: August 24, 2011
Revised: January 28, 2012
Published: January 31, 2012

   dx.doi.org/10.1021/jp2081758 | J. Phys. Chem. B 2012, 116, 2787−2800

as the rest are restricted for irrigation or human supply. However, the knowledge of these deep formations and the processes which affect CO_2 diffusion, as well as the effect of the CO_2 on the other properties of the CO_2−brine mixture, still remain poorly understood. This is why simulation models can be used to predict and understand the behavior of these systems under reservoir conditions, by considering the geochemical, hydrological, and mechanical processes that take place in reservoirs.

Reservoir simulation models are used to study the impact of CO_2 injection both in oceans and in geological formations. For the diffusion of CO_2 into deep oceans, the models more often used are box-type models.[13,14] The quantity of CO_2 dissolved in the ocean is calculated by considering the amount of CO_2 present in the atmosphere and taking into account the acid−base equilibrium of CO_2 in water. Oceans are modeled as the sum of two parts: the superficial ocean which exchanges CO_2 in an active way with the atmosphere and the deep ocean in which CO_2 diffuses. For the geological sequestration of CO_2, reactive transport models are used to describe the evolution of CO_2 in space and time scales.[15] Reactive transport modeling integrates the geochemical, hydrological, and mechanical processes that characterize dynamic geologic systems. These processes, which include chemical reactions, fluid flow, heat transfer, and mechanical stress and strain, are interdependent and must be modeled simultaneously to simulate the true behavior of geologic systems. Reservoir simulation methods require some experimental data such as solubility of CO_2 in brine mixtures and its diffusion coefficient at different thermodynamic and salinity conditions.

Determination of solubility of dissolved gases in brine is possible experimentally. However, the measurement of the diffusion coefficients of such mixtures is extremely difficult since it requires the implementation of very complex experimental protocols. Moreover, the influence of possible impurities makes experiments very difficult. As an alternative, different theoretical approaches have been used to describe mass transport in multicomponent systems. These approaches, which include hydrodynamic theory, kinetic theory, or the so-called Maxwell−Stefan (MS) equations, are, in general, of limited application. However, some authors have shown that MS relations, combined with the use of molecular simulation techniques, can provide mass transport parameters, including diffusion coefficients or electrical conductivities for systems containing an arbitrary number of species.[16−18] Therefore, molecular dynamics simulations (MD) are a good complement to experiments to determine physical properties in complex systems. In this respect, Zabala et al. have succeeded in modeling mass diffusion coefficients of CO_2−hydrocarbon mixtures at reservoir conditions by means of molecular dynamics simulations.[19]

Another way to analyze the dynamic behavior of CO_2 in brine is to explore the reorientational relaxation time of the different species in the system. Orientation relaxation dynamics of water molecules in CO_2−brine mixtures would give us indirect information about the hydrogen bond pattern and how it is affected by increasing salt concentration, temperature, and CO_2 concentration. In this context, by defining relevant vectors in water and CO_2 molecules, we can study whether rotations around some of these axes are affected by the different conditions.

The aim of this paper is to calculate CO_2 mass diffusion coefficients, as well as rotational relaxation times, in brine mixtures under the thermodynamic conditions of water reservoirs, using molecular dynamics simulations. To the best of our knowledge, a prediction of this kind has not been done yet, neither experimentally nor using simulations. Hence, our results are the first estimation of mass-diffusion and rotational relaxation times of CO_2 in deep saline aquifers. We calculate in addition the electrical conductivities of CO_2−brine mixtures under the same thermodynamic conditions and compare them to an experimental correlation available in the literature for the cases where its use is prescribed.

Finally, we propose a new method of estimation of CO_2 mass diffusion coefficients from data on rotational relaxation times that can be useful in engineering applications.

2. THEORETICAL METHODS

2.1. Diffusion. Diffusive mass transfer in mixtures can be described by Fick's law. Fick's law is a phenomenological law that relates the molar diffusion flux of a solute species (referred to as 2, the index 1 is reserved to the solvent, from now on) with the gradient of concentration for the solute species. In a binary mixture it reads

$$J_2 = -c_t D_{21} \nabla x_2 = -J_1 \tag{1}$$

where J_1 and J_2 are the solute molar diffusive fluxes; c_t is the mixture molar density; x_2 is the mole fraction of the solute; and D_{21} is the binary Fick diffusion coefficient of the mixture. This phenomenological law expresses the underlying linear relationship between the dissipative flux J_2 (more specifically the molar velocity $v_2 = J_2/c_2$, where c_2 is the molar concentration of species 2) and the conjugated thermodynamic force $-[c_2/(RT)]\nabla_{P,T}\mu_2$ where the subscripts T and P stand for constant temperature and pressure and μ_2 is the chemical potential of species 2.[20] In the multicomponent system one writes in general

$$J_i = -c_t \sum_{\substack{j=1 \\ i\neq j}}^{n} [D]_{ij} \nabla x_j \tag{2}$$

By construction, $\sum_{i=1}^{n} J_i = 0$ and $\sum_{i=1}^{n} x_i = 1$, with n being the total number of species. Moreover, $[D]_{ij}$ is the ij-element of the $(n-1)\times(n-1)$ matrix of diffusion coefficients. Equation 2 also expresses the coupling between the diffusive flux of one species with all gradients of composition. Therefore, in a binary solution, D_{21} stands for the Fick diffusion coefficient of the solute 2 in the mixture with solvent 1. From a practical point of view, the diffusion coefficients are strongly dependent functions of the thermodynamic state for nonideal mixtures. On the other hand, the Maxwell−Stefan theory that we will use along the paper considers that the thermodynamic force acting on species i is instantaneously balanced by a *mechanical friction* with the rest of the species present in the system. The frictional forces between a given pair ij of species is defined as $d_{ij} = -(x_j J_i - x_i J_j)/(c_t D_{ij}^{MS})$. Hence, the total force balance on species i reads

$$-\sum_{j\neq i} d_{ij} - \frac{x_i}{RT}\nabla_{T,P}\mu_i = 0 \tag{3}$$

The coefficients D_{ij}^{MS} are referred to as the Maxwell−Stefan coefficients, which satisfy $D_{ij}^{MS} = D_{ji}^{MS}$ due to the Onsager symmetry relations.[21] One of these equations is redundant due to the fact that $\sum_{i,j\neq i} d_{ij} = 0$, by construction, and $\sum_i (x_i)/(RT)\nabla_{T,P}\mu_i = 0$ due to the Gibbs−Duhem equation. In the

dx.doi.org/10.1021/jp2081758 | J. Phys. Chem. B 2012, 116, 2787−2800

Maxwell−Stefan theory (MS), then the equivalent to eq 2 takes the form

$$J_i = -c_t \sum_{j=2}^{n} [B^{-1}]_{ij}(x_j \nabla_{P,T}\mu_j) \tag{4}$$

where the elements of the matrix [B] are defined in terms of the phenomenological MS diffusion coefficients as follows

$$B_{ii} = \frac{x_i}{D_{i1}^{MS}} + \sum_{\substack{k=1 \\ k\neq i}}^{n} \frac{x_k}{D_{ik}^{MS}} \tag{5}$$

$$B_{ij} = -x_i\left(\frac{1}{D_{ij}^{MS}} - \frac{1}{D_{i1}^{MS}}\right), \text{ where } i, j = 2, ..., n \tag{6}$$

Then the relationship between the Fick diffusion coefficients and the MS coefficients is given through a matrix of thermodynamic factors [Q] defined as[16,21]

$$[Q]_{ij} = \delta_{ij} + x_i\left(\frac{\partial \ln \varphi_i}{\partial x_j}\right)_{T,P,\Sigma} \tag{7}$$

where φ_i is the fugacity coefficient of ith species and δ_{ij} stands for the Kronecker symbol. The subscript Σ in right-hand side of eq 7 is used to indicate that the differentiation with respect to the mole fraction x_j is to be carried out while keeping constant the mole fractions of all other species except the nth. Therefore, it is assumed that

$$[D] = [B]^{-1}[Q] \tag{8}$$

In this work, we straightforwardly determine the elements of the matrix $[B]^{-1}$ through molecular dynamics simulations. However, once $[B]^{-1}$ is known, one can obtain the matrix of Maxwell−Stefan coefficients $[D^{MS}]$ from eqs 5 and 6. Equivalently, the matrix of Fick diffusion coefficients can also be obtained from eq 8 by calculating the thermodynamic matrix [Q] from appropriate models for the fugacity coefficient φ_i using, for instance, equations of state (EOS) or thermodynamic activity coefficient models. In general, for nonideal mixtures, on one hand, [Q] is a strong function of mixture composition, while D_{ij}^{MS} is generally weakly composition-dependent. On the other hand, for the case of thermodynamic ideal liquid mixtures, $\varphi_i = 1$, and consequently, [Q] tends to the identity matrix [1]. In this last situation, in a binary mixture ($\varphi_1 \to 1$), the Fick diffusivity is equal to the MS diffusivity. In the multicomponent case, one has in this limit $[D] = [B]^{-1}$. This is also the case in a dilute solution.

From molecular dynamics simulations, MS diffusion coefficients can be calculated from the elements Λ_{ij} of an n-dimensional symmetric matrix of the so-called Onsager coefficients [Λ]. These coefficients are evaluated from the correlations in the system, according to either Generalized Einstein's relations[17]

$$\Lambda_{ij} = \frac{1}{6}\lim_{\Delta t\to\infty}\frac{1}{N}\frac{1}{\Delta t}\langle(\sum_{k=1}^{N_i}\vec{r}_{i,k}(t+\Delta t) - \sum_{k=1}^{N_i}\vec{r}_{i,k}(t))\cdot (\sum_{m=1}^{N_j}\vec{r}_{j,m}(t+\Delta t) - \sum_{m=1}^{N_j}\vec{r}_{j,m}(t))\rangle \tag{9}$$

or the equivalent Green−Kubo expressions.

$$\Lambda_{ij} = \frac{1}{3N}\int_0^\infty \langle(\sum_{k=1}^{N_i}\vec{V}_{i,k}(0)\cdot\sum_{m=1}^{N_j}\vec{V}_{j,m}(\tau))\rangle d\tau \tag{10}$$

Notice that the variables of the correlation in both eqs 9 and 10 are the baricenters of the mass distribution of each species. These expressions need not to be confused with expressions for the self-diffusion coefficients. The elements Λ_{ij} satisfy the mass balance constraint given by

$$\sum_i M_i\Lambda_{ij} = 0 \tag{11}$$

Here, $\vec{r}_{i,k}(t)$ is the center-of-mass position vector of molecule k, belonging to species i; $\vec{V}_{j,m}(t)$ is the center-of-mass velocity vector of molecule m, belonging to species j; M_i is the molecular mass of the ith species; N is the total number of molecules; and N_i is the number of molecules of the ith species.

The Onsager coefficients are related to the elements of an $(n-1)$-dimensional matrix [Δ] by[17]

$$\Delta_{ij} = (1-x_i)\left(\frac{\Lambda_{ij}}{x_j} - \frac{\Lambda_{i1}}{x_1}\right) - x_i\sum_{\substack{k=1 \\ k\neq i}}^{n}\left[\frac{\Lambda_{kj}}{x_j} - \frac{\Lambda_{k1}}{x_1}\right] \tag{12}$$

The matrix inverse of [Δ] is precisely the [B] matrix, and hence

$$[B]^{-1} = [\Delta] \tag{13}$$

For the case of binary mixtures ($n = 2$), the matrices [Δ] and [B] are scalars, and so is [Q]. Using eq 5 and remembering that $\sum_{i=1}^{n} x_i = 1$, the MS diffusion coefficient D_{12}^{MS} is obtained

$$B_{11} = \frac{1}{\Delta_{11}} = \frac{x_1}{D_{12}^{MS}} + \frac{x_2}{D_{12}^{MS}} = \frac{1}{D_{12}^{MS}} \tag{14}$$

$$\begin{aligned} D_{12}^{MS} &= \Delta_{11} \\ &= x_2\left(\frac{\Lambda_{11}}{x_1} - \frac{\Lambda_{12}}{x_2}\right) - x_1\left(\frac{\Lambda_{21}}{x_1} - \frac{\Lambda_{22}}{x_2}\right) \\ &= \frac{x_2\Lambda_{11}}{x_1} + \frac{x_1\Lambda_{22}}{x_2} - \Lambda_{12} - \Lambda_{21} \end{aligned} \tag{15}$$

The equations for ternary mixtures ($n = 3$) and quaternary mixtures ($n = 4$) are presented in the Supporting Information.

For the purpose of this article, it is interesting to consider that the system is diluted. In particular, that the mole fraction of the solvent (water) x_1 is of the order of 1 and 1 order of magnitude larger than that of the ionic species in the brine x_i, $i = 3, 4, ..., n$, which, in turn, are 1 order of magnitude larger than the mole fraction of the dissolved CO_2, x_2. Furthermore, from the definition of eq 9 we observe that $\Lambda_{ij} \propto x_i^{1/2}x_j^{1/2}$, in the limit of infinite dilution, where all molecules of the solutes diffuse independently of each other, hence uncorrelated. Therefore, in this limit, eq 9 reduces to $\Lambda_{ij} = x_i D_i^{self}\delta_{ij}$, where D_i^{self} stands for the self-diffusion coefficient. Notice that, in general, if $i \neq j$ the right-hand side of eq 9 rapidly changes sign, giving a smaller contribution than the $i = j$ case. Hence, if we denote by ε the order of magnitude of the small quantities (the mole fractions of the solutes as well as the contributions of the

dx.doi.org/10.1021/jp2081758 | J. Phys. Chem. B 2012, 116, 2787−2800

off-diagonal elements), then $\Lambda_{ij} \propto \varepsilon^2$ for $i = j$, and $\Lambda_{ij} \propto \varepsilon^3$ for $i \neq j$. We will consider that the dependent diffusive flow is that of the solvent (species 1). Notice that the particular case of Λ_{11} could be conceived as the larger term, according to the previous arguments. However, in view of eq 11, this contribution is at least of the order of $\Lambda_{i1} \propto \varepsilon^2$ with $i \neq 1$. Therefore, due the considerations just made, the off-diagonal elements of the Onsager matrix of coefficients are much smaller than the diagonal ones. The matrix $[\Delta]$ under these approximations takes the form

$$\Delta_{ij} \approx (1 - x_i)\left(\frac{\Lambda_{ii}}{x_i}\right)\delta_{ij} + \left(\frac{\Lambda_{ij}}{x_j}\right)(1 - \delta_{ij}) + O(\varepsilon^3) \tag{16}$$

Therefore, from eqs 4 and 16, up to the leading order for diagonal and off-diagonal terms, the diffusive fluxes can be written as $(i \neq 1)$

$$J_i = -c_t \sum_{j=2}^{n} \left[(1 - x_i)\left(\frac{\Lambda_{ii}}{x_i}\right)\delta_{ij} + \left(\frac{\Lambda_{ij}}{x_j}\right)(1 - \delta_{ij})\right] x_j \nabla_{P,T}\mu_j \tag{17}$$

Under this approximation, the Fick diffusion coefficients are given from eq 8 by

$$D_{ij} \cong \sum_{k=2}^{n} \left[(1 - x_i)\left(\frac{\Lambda_{ii}}{x_i}\right)\delta_{ik} + \left(\frac{\Lambda_{ik}}{x_k}\right)(1 - \delta_{ik})\right] Q_{kj} \tag{18}$$

The leading order reads

$$D_{ij} \cong \left(\frac{\Lambda_{ii}}{x_i}\right) Q_{ij} \tag{19}$$

Notice that $D_{ij} \neq D_{ji}$ for the Fick diffusion coefficients, according to the notation used along this work. This expression cannot be further approximated without an explicit knowledge of the elements of the matrix of thermodynamic factors, although in most cases it will be dominated by the diagonal elements. To obtain the MS diffusivities requires a little bit more algebra. Effectively, according to our hypothesis, the matrix $[\Delta]$ is dominated by the diagonal terms. Therefore, we can invert (left inverse) this matrix using the off-diagonal terms as a perturbation. The inverse matrix is an approximation of the $[B]$ matrix, which, up to first order, reads

$$B_{ij} \approx \frac{x_i}{\Lambda_{ii}}\delta_{ij} - \frac{x_i \Lambda_{ij}}{\Lambda_{ii}\Lambda_{jj}}(1 - \delta_{ij}) + O(\varepsilon) \tag{20}$$

On the other hand, eqs 5 and 6 can also be approximated with regard to the concentrations. Equation 5 can be approximated as

$$B_{ii} \approx \frac{x_1}{D_{i1}^{\mathrm{MS}}} + O(\varepsilon) \tag{21}$$

From this expression and from eq 20 we finally find that

$$D_{i1}^{\mathrm{MS}} \cong \frac{x_1}{x_i}\Lambda_{ii} \cong \frac{\Lambda_{ii}}{x_i} \cong D_i^{\mathrm{self}} \tag{22}$$

The last expression follows from the consideration of dilute limit in the computation of Λ_{ii}, as discussed after eq 9. This equation indicates that the element that has a larger influence in the motion of a solute i is the friction with the more abundant solvent. From eq 6, we can obtain the terms D_{ij}^{MS}, for $j \neq 1$. However, to preserve the symmetry of the matrix of Maxwell–Stefan coefficients, we derive the expression from the sum of the two elements that contain D_{ij}^{MS}, namely, B_{ij} and B_{ji}. Then, using eq 22 and the off-diagonal elements in eq 20, one obtains the approximate expression

$$D_{ij}^{\mathrm{MS}} \approx \frac{(x_i + x_j)\Lambda_{ii}\Lambda_{jj}}{\left((x_i + x_j)\Lambda_{ij} + \frac{x_i^2}{x_1}\Lambda_{jj} + \frac{x_j^2}{x_1}\Lambda_{ii}\right)}, \quad \text{where } i, j = 2, \ldots, n;\ i \neq j \tag{23}$$

To increase the accuracy of the measure, we introduce here a formal simplification of the problem through the consideration of the brine as an effective solvent, as if it were a single species. In this approximation it is implicitly considered that the relative composition of the constituents of the brine is not affected by the diffusion of the solute (CO_2, in our case). In this case, the evaluation of the Onsager matrix reduces to a 2×2 matrix, whose elements are calculated summing over all the species of the brine except CO_2 in eqs 9 or 10. One can verify that

$$\Lambda_{2b} = \sum_{i\neq 2}^{n} \Lambda_{2i} \cong \Lambda_{21}$$
$$\Lambda_{bb} = \sum_{\substack{i\neq 2 \\ j\neq 2}}^{n} \Lambda_{ij} \cong \Lambda_{11} \tag{24}$$

where the subscript b stands for brine. The element Λ_{22} remains the same. Therefore, we have verified that in the dilute limit this approximation is consistent with the more formal treatment.

As far as the diffusion coefficients are concerned, this approximation reduces the problem to the diffusion of CO_2 in the brine and, therefore, to one single Fick's and MS diffusion coefficients. Nevertheless, we have calculated the four elements of the CO_2–brine Onsager matrix for completeness.

Finally, the evaluation of the MS coefficients under dilute solution conditions is the subject of a large uncertainty if straightforwardly obtained through the Onsager elements Λ_{ij}. The fact that the latter are based on the mean square displacement of the baricenter of the species reduces the number of representative trajectories to one per simulation. However, in the dilute limit we have indicated that

$$\frac{1}{N}\langle\left(\sum_{k=1}^{N_i} \vec{r}_{i,k}(t + \Delta t) - \sum_{k=1}^{N_i} \vec{r}_{i,k}(t)\right)\cdot \left(\sum_{m=1}^{N_j} \vec{r}_{j,m}(t + \Delta t) - \sum_{m=1}^{N_j} \vec{r}_{j,m}(t)\right)\rangle \cong x_i\left(\frac{1}{N_i}\sum_{k=1}^{N_i} \langle(\vec{r}_{i,k}(t + \Delta t) - \vec{r}_{i,k}(t))^2\rangle\right)\delta_{ij} \tag{25}$$

due to the fact that the solute particles evolve independently and only products of terms referring to the same particle have a significant correlation. The approximate expression of the right-hand side of this expression is statistically more significant precisely because each individual particle trajectory can be used

dx.doi.org/10.1021/jp2081758 | J. Phys. Chem. B 2012, 116, 2787–2800

in the average. Notice, in addition, that the latter is proportional to the self-diffusion coefficient D_i^{self}, as indicated above. We will adopt this perspective in the calculation of the MS diffusion coefficients for the CO_2.

In addition to the calculation of the Onsager coefficients Λ_{ij}, related to the diffusive processes, other properties related to irreversible processes can also be obtained using the corresponding Einstein and GK formulations. An interesting quantity to obtain through MD simulations is the electrical conductivity κ, for which experimental data are available in the literature to compare with the simulation results.[18] The Einstein and GK expressions for κ are the following (eqs 26 and 27)

$$\kappa = \frac{1}{6k_BTV}\lim_{t\to\infty}\frac{d}{dt}\langle(\sum_{i=1}^{N}\hat{Q}_i\vec{r}_i^{CM}(t) - \sum_{j=1}^{N}\hat{Q}_j\vec{r}_j^{CM}(0))^2\rangle \quad (26)$$

$$\kappa = \frac{1}{3k_BTV}\int_0^\infty\langle(\sum_{i=1}^{N}\hat{Q}_i\vec{V}_i^{CM}(\tau))\cdot(\sum_{j=1}^{N}\hat{Q}_j\vec{V}_j^{CM}(0))\rangle d\tau \quad (27)$$

where $\hat{Q}_i = \sum_{j=1}^{n_i} q_j$, and $\vec{r}_i^{CM}$ and $\vec{V}_j^{CM}$ are, respectively, the total net charge, the center of mass position, and velocity of the total N molecules/ions in the system (n_i is the number of atoms of a molecule i).

2.2. Reorientational Dynamics. The rotational dynamics of water and CO_2 molecules in brine can be analyzed through temperature-dependent reorientational relaxation times. For water, the H−H and O−H relaxation can be obtained from ^{1}H−^{1}H and ^{17}O−^{1}H dipole relaxation NMR experiments. The correlation function of the dipolar moment of water is experimentally obtained from optical measurements (Raman scattering, fluorescence depolarization, and Kerr relaxation experiments).[22] For CO_2, O═C═O relaxation can be determined by ^{13}C and ^{17}O NMR longitudinal relaxation times in conjunction with microwave spectroscopy at a wide range of pressures and temperatures.[23−25] Depolarized Rayleigh scattering measurements have also been applied by Versmold to study the molecular reorientation of CO_2.[26]

We have computed the reorientational correlation time of several unit vectors, depending on the geometry of the molecule. In the case of water, three vectors are defined, i.e., joining the two hydrogen atoms (H−H), the dipole moment (μ), and a vector perpendicular ($\perp$) to the plane of the molecule. For CO_2 only the vector aligned to the C═O bond is considered. The orientational autocorrelation functions can be defined as

$$C_i^l(t) = \langle P_l(\hat{\mathbf{e}}_i(t)\cdot\hat{\mathbf{e}}_i(0))\rangle \quad (28)$$

where P_l is a Legendre polynomial with l = 1,2 for first and second order, respectively and $\hat{\mathbf{e}}_i$ is one of the aforementioned unit vectors. These functions are commonly fitted to Kohlrausch−Williams−Watts exponential functions[27,28]

$$C_{i,KWW}^l(t) = \exp[(-t/\alpha_i^l)^{\beta_i^l}] \quad (29)$$

for which the relaxation time can be obtained through

$$\tau_i^l = \int_0^\infty C_{i,KWW}^l(t)dt = \frac{\alpha_i^l}{\beta_i^l}\Gamma\left(\frac{1}{\beta_i^l}\right) \quad (30)$$

2.3. Soreide and Whitson Thermodynamic Model for Electrolyte Solutions. The thermodynamic factor Q has been estimated through the Soreide and Whitson equation of state (EOS) model.[29] This is an extension of the Peng−Robinson model that is adapted for the salt water system. The CO_2 fugacity coefficient ($\ln\varphi_2$) at a given composition is obtained at the bubble pressure as calculated by the EOS at the same pressure and temperature. To numerically compute the derivative in eq 7, we slightly vary the mole fraction by an increment of $\Delta x_2 = 10^{-5}$ to the actual mole fraction.

3. SIMULATION METHODS

Molecular dynamics simulations were performed using the DLPOLY v2.19 code. The different properties computed have been obtained by post-treatment of trajectories generated with this code. Both water and carbon dioxide were treated as rigid molecules using pair potentials composed of Lennard-Jones (LJ) and Coulombic terms (eq 31). The SPC/E model[30] was used for water−water interactions as it correctly reproduces transport, thermodynamic, and structural properties of water better than other available models in the literature[31] but also because it has been widely used for modeling aqueous ionic solutions.[18,32−35] Carbon dioxide was treated as a rigid molecule with a quadrupole charge using the EPM2 intermolecular potential.[36] Na/Cl atoms were also described by LJ interaction centers plus point charges to describe the electrostatic interactions with the rest of the molecules in the system. For the ions we have used the optimized potential of Wheeler and Newman[18] since it better reproduces the density ionic-aqueous solutions than the intermolecular model derived by Dang.[37] The LJ parameters for the different species are shown in Table 1.

Table 1. Intermolecular Potential of the SPC/E Model of H_2O and the EPM2[36] Model of CO_2, Na^+, and Cl^-

H_2O		
bond distance (Å)	D(O−H)	1.000
angle (°)	θ(H−O−H)	109.4
atom (group)	O	H
M (g/mol)	15.9994	1.00794
ε (kJ/mol)	0.650	0
σ (Å)	3.166	0
q (e)	−0.8476	0.4238
CO_2		
bond distance (Å)	D(C−O)	1.149
atom (group)	C	O
M (g/mol)	12.0107	15.9994
ε (kJ/mol)	0.2339	0.6693
σ (Å)	2.757	3.033
δ (Å)	0	0
q (e)	0.6512	−0.3256
Ions		
atom (group)	Na^+	Cl^-
M (g/mol)	22.9898	35.4530
ε (kJ/mol)	0.45980	0.45064
σ (Å)	2.35	4.42
q (e)	1.0	−1.0

The long-ranged electrostatic interactions described in eq 31 were treated by the Ewald summation technique with a

dx.doi.org/10.1021/jp2081758 | J. Phys. Chem. B 2012, 116, 2787−2800

tolerance of 10^{-6} in the electrostatic energy. Crossed LJ interactions between the different force field centers were computed using the Lorentz−Berthelot mixing rules as described by eqs 32 and 33

$$U_{ij} = \underbrace{4\varepsilon_{ij}\left[\left(\frac{\sigma_{ij}}{r_{ij}}\right)^{12} - \left(\frac{\sigma_{ij}}{r_{ij}}\right)^{6}\right]}_{\text{Lennard−Jones term}} + \underbrace{\sum_{\substack{i,j \\ i<j}} \frac{1}{4\pi\varepsilon_0}\frac{q_i q_j}{r_{ij}}}_{\text{Electrostatic term}} \tag{31}$$

$$\varepsilon_{ij} = \sqrt{\varepsilon_i \varepsilon_j} \tag{32}$$

$$\sigma_{ij} = \frac{\sigma_i + \sigma_j}{2} \tag{33}$$

where ε_{ij} and σ_{ij} are the Lennard-Jones parameters between centers i and j; q_i and q_j are the point charges of sites i and j; ε_0 is the permittivity of the vacuum; and $r_{ij} = |r_j - r_i|$ is the distance between sites i and j.

The Verlet leapfrog algorithm has been used to integrate the equations of motion with a time step of 2 fs and a cutoff distance of 12.5 Å for all cases. A Verlet list with a second cutoff radius of 13.5 Å was used to improve CPU time. The rotational part of the equations of motion was integrated using the Fincham implicit quaternion algorithm[38] with a quaternion tolerance of 10^{-8}. All the MD simulations were carried out in cubic boxes with periodic boundary conditions. The number of molecules of water for all the simulations was in the range of 3000−3200. The number of ions used in our simulations was determined by the molality concentration of the solution, and the number of molecules of CO_2 was determined by the saturation concentration at the desired temperature, pressure, and molality, according to the experimental values.[39] To determine the density of the mixture and, therefore, the box size for the different systems, NPT simulations using the Nosé−Hoover thermostat-barostat were carried out before production runs. The relaxations times, τ_T and τ_P, controlling temperature and pressure fluctuations, are 0.1 and 1.0 ps, respectively. For equilibration and production runs, the NVT−Nosé−Hoover ensemble was used with τ_T equal to 0.1 ps. For all the systems, the positions and the velocities for each atom on each molecule were stored every 20 time steps. To obtain the density of the mixture, NPT runs of 25×10^4 time steps were carried out. Equilibration runs were also done with 25×10^4 time steps, while productions runs were done with 75×10^4 time steps. Statistical uncertainties of the diffusion coefficient are estimated from several runs starting at different independent initial conditions. We found values that are strongly dependent on the system's composition and on the nature of the coefficient, namely, 10−15% for the self-diffusion coefficient and 10−50% for the mutual diffusion coefficient.

Production trajectories were analyzed with the post-treatment code to compute MS diffusion coefficients through eqs 5, 6, and 9−13. Electrical conductivity is calculated through eqs 26 and 27 and rotational dynamics through eqs 28 and 29. To validate the accuracy of the selected force fields, several simulations were done before considering the case of CO_2 in brine. First, MS diffusivity of NaCl ions in water was determined at different molal concentrations and compared to both simulation and experimental values.[18] Second, binary MS diffusion coefficients of CO_2 in water were computed and compared to the available experimental data in the literature, at atmospheric pressure and for several temperatures.[40−43] Due to the low solubility of CO_2 in water or in brine, all simulations were performed with the mole fraction of CO_2 greater than or equal to 10^{-3}. This implies that one has, at least, 10 molecules of CO_2 on each simulation box, which is a small number. One important consequence of the low solubility of this gas in water at ambient conditions is the lack of statistical significance of the data, which is translated into large error bars in the evaluation of the terms $\Lambda_{CO2-CO2}$ and $\Lambda_{H2O-CO2}$, defined in eqs 9 and 10, even for quite long simulation runs (1.5 ns). This fact makes it difficult to compare the simulation results with experiments at pressures close to the ambient conditions. However, as we have pointed out in Section 2, $\Lambda_{CO2-CO2}$ is well approximated by the self-diffusion coefficient, whose calculation is much more precise than the straightforward use of eq 9. For $\Lambda_{H2O-CO2}$, however, no simple approximation like the former exists. Additional calculations were done for MS diffusivity of CO_2 in water at different temperatures and pressures up to 1000 bar. In this region, the CO_2 mole fractions are of the order of 10^{-2}. The selected thermodynamic conditions of the different systems studied are summarized in Table 2, Table 3, and Table 4.

Table 2. Comparison of the Simulation Results for the Electrical Conductivity for Na−Cl−Water Systems at Different Salt Concentrations (m) and 298.15 K with the Experimental Data and Simulation Results of Wheeler and Newman

conc. (m)	no. ions	$\kappa_{exp.}$ (S/cm)	κ_{calc}, this work GK/Einst. (S/cm)/dev.exp.	κ_{calc} Wheeler & New. (S/cm)/dev·exp
1	54	0.076	0.085/0.082	0.073
			11.8%/7.9%	4.0%
2	135	0.159	0.137/0.117	0.104
			13.8%/26.4%	34.6%
4	216	0.212	0.159/0.158	0.119
			25.0%/25.5%	43.9%

As a first approximation, for the CO_2 dissolved on pure water, especially at ambient conditions, we have that the thermodynamic factor is approximately equal to 1 since the mole fraction of CO_2 is very small in all the systems analyzed. Consequently, the binary Fick diffusion coefficient can directly be approximated by the MS diffusivity and thus compared to the available experimental data for this property at ambient pressure. Otherwise, one can use eq 19 as valid in the dilute limit. Unfortunately, experimental data for diffusion coefficients at pressures higher than the atmospheric pressure are lacking. Instead, as we are not far from infinite dilution of CO_2 in water, we can use a widely known correlation to estimate the diffusivity in nonelectrolyte solutions to later compare to our simulation results at higher pressures. The correlation used is the Wilke−Chang equation[44]

$$D_{AB}^{0} = 7.4 \times 10^{-8}\frac{(\phi \cdot M_B)^{1/2} T}{\eta_B V_A^{0.6}} \tag{34}$$

where D_{AB}^{0} is the mutual diffusion coefficient of the solute A at very low concentration in the solvent B; M_B is the molecular mass of solvent B; T is the temperature; η_B is the viscosity of the solvent; V_A is the molar volume of the solute at its boiling point; and ϕ is a dimensionless parameter referred to as association factor. If the solvent is water, the recommended

dx.doi.org/10.1021/jp2081758 | J. Phys. Chem. B 2012, 116, 2787−2800

Table 3. Comparison of the Simulation Results for the MS Diffusion Coefficient for CO_2−Water Systems at P = 1.013 bar and Different Temperatures with the Experimental Data in the Literature[49,50,a,b]

T (K)	no. CO_2 molecules	no. water molecules	ρ_{avg} (g/cm^3)	$D_{22exp.}$ (10^{-9} m^2/s)	D_{22calc}, this work, GK/Einst. (10^{-9} m^2/s)/std.dev.
283.15	3	3175	1.005	1.46	1.82/1.83
					0.27/0.43
298.15	2	3250	0.998	1.98	1.98/2.04
					0.19/0.36

[a]The simulation data are obtained through NVT simulations after NPT simulations at P = 1.013 bar have been used to determine the actual density. [b]Here, we have considered $D_{22}^{Fick} = D_{12}^{MS}$ since the thermodynamic factor $Q \approx 1$ for the conditions studied.

Table 4. Comparison of the Simulation Results for the MS Diffusion Coefficient for CO_2−Water Systems at P > 1.013 bar and Different Temperatures with the Wilke−Chang Correlation[44,a]

therm. cond. T (K)/P (bar)	no. CO_2 molecules	ρ_{avg} (g/cm^3)	$D_{12\ calc}$, Wilke− Chang (10^{-9} m^2/s)	$D_{12\ calc}^{MS}$, this work GK/Einst. (10^{-9} m^2/s)/std. dev.	Q_{22} factor	D_{12} Fick GK/Einst. (10^{-9} m^2/s)
303.15/100	73	1.014	2.19	2.55/2.80	0.768	1.96/2.15
				0.10/0.41		
303.15/1000	120	1.060	2.16	1.90/1.87	0.644	1.22/1.20
				0.18/0.25		
333.15/100	55	0.990	4.09	3.40/3.30	0.815	2.77/2.69
				0.06/0.44		
333.15/1000	103	1.037	3.90	2.85/2.76	0.679	1.93/1.87
				0.06/0.24		

[a]For the data obtained from the Green−Kubo and the Einstein relation method, there are significant deviations between our predictions and those obtained from the aforementioned correlation. It is, however, remarkable that the simulated data for the MS diffusion coefficients are closer to the correlation than the Fick's counterparts.

value for ϕ is 2.26.[45] The molar volume V_A can be estimated using the Tyn and Calus method[46]

$$V_A = 0.285 \cdot V_C^{1.048} \quad (35)$$

where V_C is the critical molar volume.

Simulated electrical conductivity for CO_2−brine mixtures at some thermodynamic conditions was compared to a correlation from Fleury and Deschamps.[47] Fleury and Deschamps proposed the following relationship describing the effect of dissolved CO_2 on electrical conductivity κ of aqueous NaCl solutions.

$$\kappa_S(x_{CO_2}, T) = \kappa_S(0, T_0)(1 - 6x_{CO_2})\left(\frac{T + 19.5}{T_0 + 19.5}\right) (T \text{ in } °C) \quad (36)$$

where $\kappa_S(0,T_0)$ is the electrical conductivity of aqueous NaCl solution at a reference temperature T_0 when x_{CO2} is equal to zero. This equation is valid if the temperature ranges between 35 and 100 °C.

Finally, to the best of our knowledge, there are no experimental data for comparison for reorientational dynamics of CO_2 dissolved neither in water nor in brine.

4. RESULTS AND DISCUSSION

4.1.1. Validation of the Intermolecular Potentials.

Calculation of MS Diffusion Coefficients of the Ions and the Electrical Conductivity of Brine. To test the accuracy of the Na/Cl and water intermolecular potentials, we performed NPT MD simulations for aqueous NaCl solutions at different salt concentrations to compute solution densities, MS diffusion coefficients, and electrical conductivity. The MD simulation results were compared to simulation results of Wheeler and Newman[18] and experimental data based on Chapman's fits of a compilation of experiments.[48] First of all, and before adopting a set of LJ parameters for ions, NPT MD simulations at T = 298.15 K and P = 1.01325 bar were performed to obtain solution densities. The first set of LJ parameters were those of Dang,[37] and the second were the LJ parameters provided by Wheeler and Newman.[18] Three salt concentrations were chosen for the validation test: 1, 2.5 and 4 *m*.

Figure 1 gives the simulated and experimental electrolyte solution densities as a function of molal concentration. We can

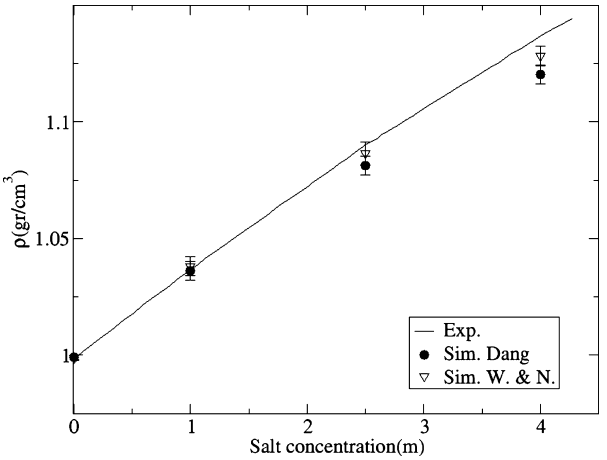

Figure 1. Simulated and experimental solution densities as a function of salt concentration. Dark circles and empty triangles correspond to solution densities calculated using Dang[37] and Wheeler and Newman[18] potentials for ions, respectively. Experimental data from ref 48.

observe that all force fields accurately reproduce the experimental solution densities for low salt concentrations within the error bars. At high salt concentrations (4 *m*), however, simulations using the Wheeler and Newman (WN) parameters reproduce better the experimental solution density

dx.doi.org/10.1021/jp2081758 | J. Phys. Chem. B 2012, 116, 2787−2800

than the Dang model. Hence, we decided to choose the WN potential to simulate Na^+ and Cl^- ions.

MS diffusion coefficients were calculated using the Einstein and GK formulations yielding the adequate Onsager's matrices, Λ_{ij}, defined in eq 9. As shown in Figure 2, for the cases Na−H_2O and Cl−H_2O, the diffusion coefficients obtained compare well with the earlier simulation results given by Wheeler and Newman,[18] although the latter are in semiquantitative agreement with experimental data. Only $D^{MS}_{Na^+-H2O}$ for a concentration of 4 *m* presents a significant deviation with respect to the experimental data larger than the 25%. As discussed in Section 2.1, $D^{MS}_{Na^+-H2O}$ and $D^{MS}_{Cl^-H2O}$ are the more relevant coefficients for the system since they are related to the friction of the ion with the surrounding solvent. For completeness, we also estimate $D^{MS}_{Na^+-Cl^-}$ despite the small value and the large uncertainty of the data. Thus, we cannot be conclusive with the $D^{MS}_{Na^+-Cl^-}$ opposite trend observed for this magnitude with respect to the salt concentration as compared to the experimental data. We have also verified that the mass balance constraint (eq 6) was satisfied (the computed value is of the order of 10^{-4}, which is acceptable considering the large fluctuations observed in the calculations of the elements of the Onsager matrix [Λ]). Full comparison of the obtained MS diffusion coefficients using either GK or Einstein formulations with experimental data and Wheeler and Newman simulations is given in the Table A1 of the Supporting Information.

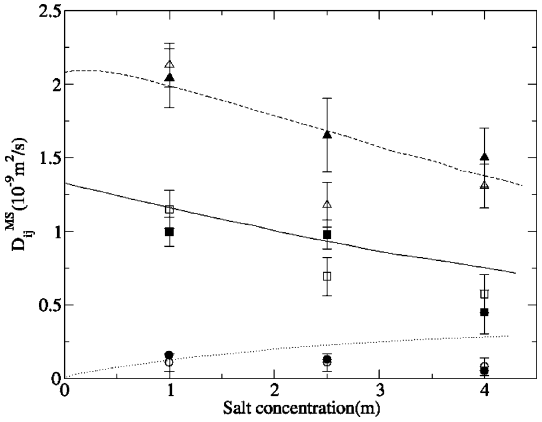

Figure 2. Simulated and experimental MS diffusion coefficients for Na−Cl−water systems as a function of salt concentration. Lines correspond to experimental data;[48] empty symbols correspond to the simulated MS diffusion coefficients obtained by Wheeler and Newman;[18] and full symbols correspond to our calculation using GK formalism. Circles and dotted line correspond to Na−Cl results; squares and solid line correspond to water−Na results; while triangles and dashed line correspond to water−Cl results.

The last property calculated for our validation test was the electrical conductivity κ. Our simulation results are shown in Table 2 and in Figure 3. Simulations underpredict the experimental conductivity mainly for high salt concentrations. This trend was also observed by Wheeler and Newman.[18] Electrical conductivity is a property that is precisely very sensitive to ion−ion interactions. Together with the previous results on the MS diffusion coefficients, the values obtained for the electrical conductivity confirm that it is likely that the chosen potentials for water and ions imply either too strong ion−ion interactions or too weak H_2O−ion interactions. The polarizability of water and ions at high ion concentration, disregarded in the models used along this work, can be the origin of the observed discrepancies, although this analysis lies outside the scope of the present work.

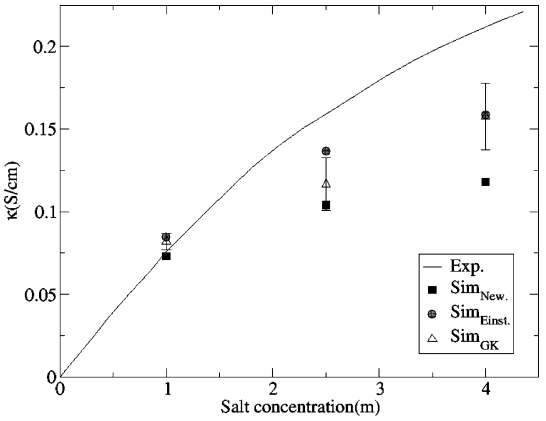

Figure 3. Simulated and experimental[48] electrical conductivities for Na−Cl−water systems as a function of salt concentration. Dark squares correspond to the simulation results of Wheeler and Newman,[18] while gray circles and empty triangles correspond to our calculation using Einstein and GK formalisms, respectively.

4.1.2. Calculation of MS Diffusion Coefficients for CO_2−Water Mixtures. We have computed the MS diffusion coefficient of CO_2 in water at different thermodynamic conditions to explore the accuracy of the EPM2 potential for CO_2 with regard to this property. In a first step, we performed NVT MD simulations with a simulation pressure P = 1.013 bar (atmospheric pressure) and T = 283.15 and 298.15 K. Experimental data at atmospheric pressure are available in the literature.[49,50] The number of molecules of CO_2 to be introduced in the simulation box was determined from experimental data on the saturation concentration at the desired temperature and pressure. As the CO_2 mole fraction is very small under the conditions of interest, three MD simulations, taking different initial conditions, were performed to average the obtained MS diffusion coefficient and to reduce the statistical uncertainty. As we are at low pressure and small solute mole fraction, the binary Fick diffusion coefficients for CO_2 can be well approximated by the corresponding MS coefficient since the thermodynamic factor Q is almost 1 under these thermodynamic conditions (it is calculated as 0.991 at 283.15 K and 0.994 at 298.15 K). Diamond et al. have recently estimated, using a large collection of experimental data, that this assumption is correct if the mole fraction of CO_2 is below 2%.[51] Hence, as it follows from eq 8 and eq 19, $D_{22} \cong \Lambda_{22}/x_2 \cong D_{21}^{MS}$. This equation indicates that, on the one hand, in dilute solution the Fick diffusion coefficient is approximately given by the self-correlation function of the solute and, on the other, that the friction (represented by the inverse of the MS coefficient) is that of the solute with the solvent.

The thermodynamic conditions and simulation results are shown in Table 3. Despite the statistical uncertainty due to the small CO_2 mole fraction, we can consider that our simulation results are in rather good agreement with the experimental data. For the case of 283.15 K, we obtained, however, a non-negligible deviation of 25% from the experimental value, which is an acceptable result considering the small number of CO_2 molecules and the length of the simulation, 1.5 ns, which yields a statistical uncertainty of 14.8% and 23.49% using the Einstein and GK formulations, respectively. Uncertainty could be reduced by increasing the size of the system keeping the

dx.doi.org/10.1021/jp2081758 | J. Phys. Chem. B 2012, 116, 2787−2800

density constant, but our system already relied on the limit of a reasonable use of the computational resources (20 molecules of CO_2 correspond to 32 500 molecules of water). However, in view of the simulation results, part of the discrepancy could be also due to inadequacies of the intermolecular potentials used.

Due to the fact that the system is diluted and that we expect the solute−solute interactions to be small, one can increase the number of CO_2 molecules by increasing the pressure of the system up to 1000 bar (yielding a ratio of about 100 CO_2 molecules to 3000 water molecules), without significantly affecting the dynamic results. Due to the lack of experimental data to compare to, we have used the well-known Wilke−Chang correlation[44] to obtain an estimate of the diffusion coefficients at the selected temperatures and pressures (see eq 34). The Wilke−Chang correlation gives, however, the diffusion coefficient at infinite dilution. In our simulations, the CO_2 mole fractions are always less than or equal to 10^{-2}, and therefore we are under the conditions of validity of the Wilke−Chang correlation. Thermodynamic conditions and simulation results as compared to Wilke−Chang predictions are shown in Table 4. For the estimate of the latter, viscosities of water at the different thermodynamic pressures and the molar volume of CO_2 at its boiling point were obtained from the NIST database.[10]

In general, we observe that the MS as well as Fick diffusivities increase when increasing the temperature and decrease when increasing the pressure. This was the intuitively expected trend, also followed by the diffusion coefficients obtained from the Wilke−Chang correlation. However, the correlation data show that there is not a strong dependence of the diffusion coefficient with pressure, due to the fact that the density is the most important factor at constant temperature. At very high pressure the local structure of water is furthermore altered, and thus it affects the diffusivities, although this factor seems to have only a weak effect in the range of pressures studied. On the other hand, in our simulations there is a reduction of about 15−30% of the MS coefficient when the pressure is increased from 100 to 1000 bar. This fact can be the consequence of an overestimation of the CO_2−H_2O interactions. In fact, Lisal et al. have noticed that the CO_2 solubility in water obtained with the EPM2 and SPC/E model overestimates the experimental values.[52] These authors attribute this behavior to a too strong CO_2−H_2O interaction. Anyway, in the comparison of the Wilke−Chang diffusivities with the simulated MS diffusivities, the average deviation is about 17%. However, the estimated values for the Fick diffusion coefficients from our simulations are in larger disagreement with the Wilke−Chang correlation, except for the initial value, at 303.15 K and 100 bar. The fact that the Wilke−Chang correlation does not contain any dependence on activity coefficients suggests that these values should better follow the trends of the MS diffusivities than Fick's diffusivities, as we observe.

4.2. Study of CO_2−Brine Mixtures. Once the accuracy of chosen potentials for different species was checked, we could proceed to the simulation of the CO_2−brine mixtures. We have performed MD simulations at thermodynamic conditions representative of deep saline aquifers, in temperature ranges from 333.15 to 453.15 K and pressure from 50 to 500 bar. Three Na/Cl molal concentrations were chosen: 1, 2, and 4 *m*. The number of CO_2 molecules at each thermodynamic condition is given in Tables B1−B9 of the Supporting Information and ranges from about 10 molecules at lower pressure to 100 at the higher pressures. The corresponding CO_2 mole fractions range from 10^{-3} to 3×10^{-2}. It is important to bear in mind that, according to experiments, the CO_2 mole fraction increases by increasing the pressure and by decreasing salt concentration.

4.2.1. Calculation of Solution Densities of CO_2−Brine Mixtures. To obtain solution densities of the mixtures for the different *P* and *T* thermodynamic conditions, NPT MD simulations were performed. Figure 4 gives the simulated densities of the mixture CO_2 + brine as a function of pressure for all considered temperatures and salt concentrations. Simulation results show that solution densities increase by increasing the pressure and salt concentration and decrease by increasing temperature. These are all expected trends. Only a few studies measuring solution densities of CO_2 + brine systems can be found in the literature. For instance, Li et al.[11] measured densities for binary systems of CO_2 + Weyburn formation brine at a temperature of 332.15 K and pressures similar to those of our study. Weyburn formation brine contains more dissolved species than present in our simulations, like calcium, magnesium, or potassium. In this case, sodium and chloride ions are the major ionic species, with molal concentrations of 1.27 and 1.48 *m*, respectively, with a measured solution density, at 333.15 K and 101.4 bar, equal to 1.0555 g/cm^3. Simulation results at a similar temperature and pressure (333.15 K and 100 bar) and salt concentrations (1 and 2 *m*) yield 1.0232 and 1.0538 g/cm^3, respectively. If we considered NaCl salt concentrations similar to those present in Weyburn formation brine, we would expect a CO_2−brine solution density around 1.039 g/cm^3. However, as we said before, Weyburn formation brine contains also species with larger molecular masses than Na^+ and Cl^-. Hence, a larger solution density than in our simulation is expected when comparing with experimental data.[11]

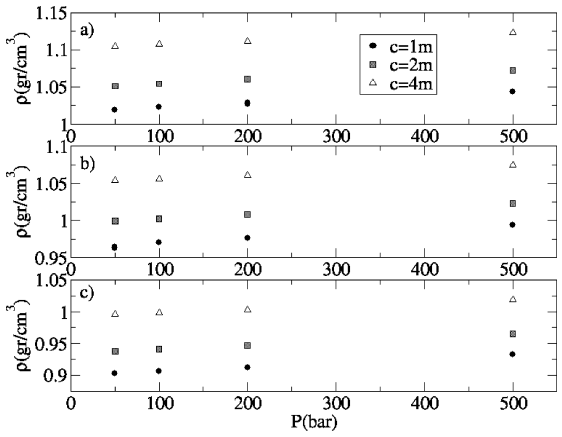

Figure 4. Simulated solution densities for CO_2−brine systems at (a) *T* = 333.15 K, (b) 393.15 K, and (c) 453.15 K as a function of pressure and for different salt concentrations.

4.2.2. MS Diffusion Coefficient of CO_2 in Brine. MS diffusion coefficients at selected thermodynamic conditions were obtained using both Einstein and GK formulations. Once the NVT MD simulations were performed, trajectories were post-treated obtaining the different MS diffusivities. To reduce the uncertainty of the results, two simulations were carried out at each thermodynamic condition, and final MS diffusivities were obtained by averaging the two values obtained after post-treatment. As indicated in Section 2.1, the MS diffusion coefficient of CO_2 in such brine is obtained from the

dx.doi.org/10.1021/jp2081758 | J. Phys. Chem. B 2012, 116, 2787−2800

computation of Λ_{22}, according to eqs 9 (conversely, 10) and 22. In the following, we analyze the more relevant trends.

Temperature and Salt Concentration Dependence of MS Diffusion Coefficients. MS diffusivity of CO_2 in brine was obtained as a function of temperature for different pressures and salt concentrations. Simulation results at 100 and 200 bar using Einstein relations based on the evaluation of the self-diffusion coefficient are shown in Figure 6. Data are listed in

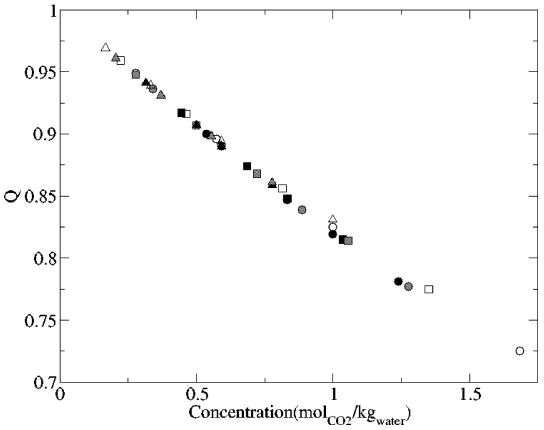

Figure 5. Variation of the thermodynamic factor Q of CO_2 in brine in function of the temperature, pressure, and salt concentration. Full symbols correspond to T = 333.15 K, gray symbols to T = 393.15 K, and empty symbols to T = 453.15 K. Circles correspond to c = 1 m, squares to c = 2 m, and triangles to c = 4 m.

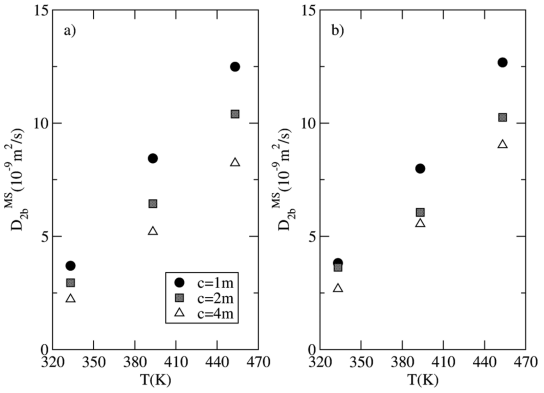

Figure 6. Simulated MS diffusion coefficients of CO_2 in brine as a function of temperature at (a) P = 100 bar and (b) P = 200 bar and for different salt concentrations. The MS diffusivities have been calculated from the self-diffusion coefficient, using Einstein formulation, as seen in eq 22. The error bars are of the order of the 10^{-12}–10^{-13} m^2/s for all the simulated conditions.

Tables B1–B9 of the Supporting Information. For all pressures, MS diffusivities increase with temperature, which was the expected trend. In addition, we observe that D_{2b}^{MS} decreases as increasing salt concentration and that the pressure of CO_2 (number of particles) plays almost an irrelevant role at this dilution. These results are consistent with these found from the direct application of eq 9 (not shown due to the large error bars).

The calculation of the thermodynamic factor Q for all studied conditions shows values that are greater than 0.78, as can be seen in Figure 5, which means that the CO_2 behaves almost ideally from a thermodynamic point of view, and therefore, the Fick diffusion coefficient D_{22} is very close to the MS diffusion coefficient although slightly smaller (results given in Tables B1–B9 of the Supporting Information). Consequently, from now on, we will only discuss the behavior of the MS diffusion coefficient.

4.2.3. Electrical Conductivity of CO_2–Brine Mixtures. Together with the inherent interest of the electrical conductivity of these CO_2–brine mixtures, the evaluation of this quantity constitutes a good test of the accuracy of the simulations as well as of the predictive behavior of the potential used for the CO_2. We hence proceed to the analysis of this property. Figure 7a gives the simulated electrical conductivity as

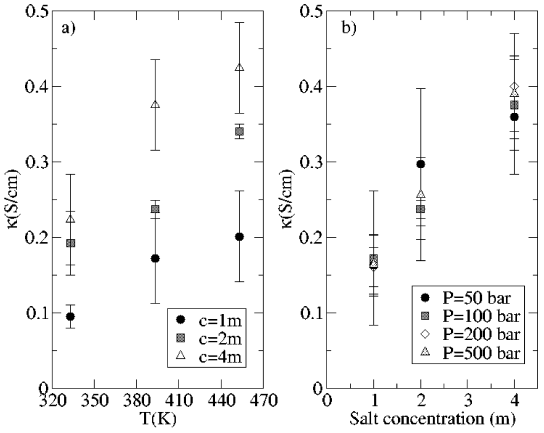

Figure 7. Simulated electrical conductivity for CO_2–brine mixtures as a function of temperature at P = 100 bar for different salt concentrations (a) and simulated electrical conductivity for CO_2–brine mixtures as a function of salt concentration at T = 393.15 K (b) for different pressures. Results were obtained using the Einstein formulation.

a function of temperature at P = 100 bar for different salt concentration using the Einstein formulation. As observed for D_{2b}^{MS}, the electrical conductivity increases with increasing temperature. This effect has been observed for all pressures. Such a behavior is expected in view of the decrease of the viscosity of the solution (mostly water) with increasing temperature. Thus, the mobility of the charge carriers increases inversely proportional to water viscosity.

As expected due to the increase of the charge carriers in the solution, the electrical conductivity increases with increasing salt concentration, as shown in Figure 7b. This trend can be clearly observed for all pressures, even for P = 50 bar, where a large dispersion in the values of MS diffusivities was obtained. No pressure dependence for electrical conductivity is observed from simulation results inside the range of certainty. The effect is weak in the high dilution limit of the dissolved CO_2. Effectively, the decrease of the conductivity with the pressure should be proportional to the decrease of the mole fractions of the conducting species due to the increase of the dissolved gas in the system. This effect would dominate over any other effect on the structure of a rather incompressible fluid due to the pressure in the range of values studied. Simulated electrical conductivities at T = 333.15 K and at salt concentration equal to 1 and 2 m can be compared to the values obtained using Fleury–Deschamps correlation (see eq 36), which reflects such a decrease of the conductivity with the increase of the pressure.

4.2.4. Rotational Relaxation Time of CO_2 and Water in Brine. The last property analyzed was the relaxation dynamics of water and CO_2 molecules from the dynamic behavior of

dx.doi.org/10.1021/jp2081758 | J. Phys. Chem. B 2012, 116, 2787–2800

several vectors defined in Section 2.2. The variation of the relaxation times $\tau_{H-H}^{1,2}$, $\tau_{\mu}^{1,2}$, and $\tau_{\perp}^{1,2}$, as defined in eq 29, with the temperature at different salt concentrations at 100 bar can be observed in Figure 8, and the data are listed in the

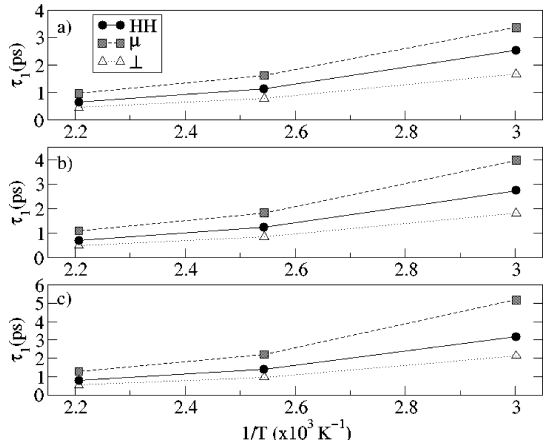

Figure 8. Variation of relaxation times of the different vectors defined for water molecules as a function of temperature and salt concentrations at 100 bar and at c = 1 m (a), c = 2 m (b), and c = 4 m (c). Only results for the Legendre polynomial of grade 1 are shown. The error bars are of the order of the size of the symbol.

Supporting Information, Tables D1−D3. We have chosen a fixed pressure to perform our calculations since neither D_{2b}^{MS} nor any of the rotational relaxation times for CO_2 seem to be a function of pressure, according to our results of the previous section. We can notice that $\tau_{\mu}^{1} > \tau_{H-H}^{1} > \tau_{\perp}^{1}$, and $\tau_{H-H}^{2} > \tau_{\mu}^{2} > \tau_{\perp}^{2}$ for all conditions investigated. The same ordering is observed in liquid water at standard conditions.[53,54] We also observe that all relaxation times increase when temperature decreases or salt concentration increases.[55,56] In fact, when temperature is kept constant, all relaxation times are almost linear functions of salt concentration (figure not shown). From Figure 8 we have extracted, by means of an Arrhenius fitting ($\tau = A \exp(\Delta E/RT)$), the activation energy (ΔE) for the three different relaxation times. On one hand ΔE_{H-H} (~14.7 kJ/mol) and $\Delta E_{\perp}$ (~13.8 kJ/mol) are weakly affected by ion concentration. On the other hand ΔE_{μ} clearly increases with salt concentration (~13−15 kJ/mol). This fact is expected since τ_{μ} reflects the relaxation time of the dipole moment of water molecules, which are strongly perturbed by the increment of ion concentration. Finally, the relaxation time of the bond vector for CO_2 at different temperatures and salt concentrations can be seen in Figure 9. We can observe an increase of the relaxation time with the decrease of the temperature. As in water molecules, $\tau_{C=O}$ also increases with the salt concentration, reflecting the overall slowing down of the dynamic of the system.

4.2.5. Prediction of the Maxwell−Stefan Mutual Diffusion Coefficients of CO_2 in Brine from Rotational Relaxation Times and Self-Diffusivity Data. We have seen so far that the main problem in obtaining the MS diffusion coefficient of CO_2 in water (either experimentally or by computer simulation) is its low solubility. The small number of molecules makes the baricenter of the CO_2 strongly fluctuate in the derivation of the appropriate Onsager coefficient, according to eq 9. In this section we will propose an alternative way to estimate D_{2b}^{MS} in

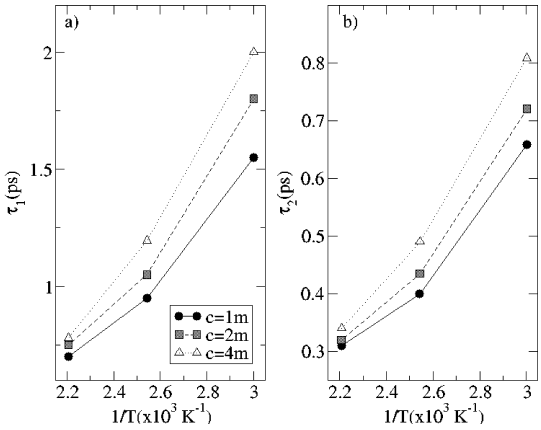

Figure 9. Variation of relaxation time for the C═O bond vector as a function of temperature and salt concentrations at 100 bar. Results for the Legendre polynomial of grade 1 (a) and 2 (b). The error bars are of the order of the symbol size.

brine from the measurement of the rotational relaxation time and, ultimately, from state variables of easy access.

Together with the direct determination of the diffusion coefficient, one can estimate D_{2b}^{MS} by using several correlations such as that of Darken

$$D_{2b}^{MS} = x_2 D_b^{self} + x_b D_2^{self} \cong x_b D_2^{self} \quad (37)$$

where D_i^{self} stands for the self-diffusion coefficients of the species i.[57] The second is valid in the limit of high dilution of CO_2. One also has the Cadwell and Babb approximation for D_{2b}^{MS}, which relies on a linear combination of the diffusion coefficient of species i evaluated at infinite dilution, namely, D_i^{∞} ($D_{2b}^{MS} = x_2 D_b^{\infty} + x_b D_2^{\infty}$).[58] It is known that the Darken relation gives a reasonable prediction of the mutual diffusion coefficient, particularly when one component is close to infinite dilution, which is the case of CO_2 in brine. This is in agreement with what we have derived in our analysis of Section 2.1. In this sense, the Cadwell and Babb relation neglects the fact that the MS diffusion coefficient is usually nonideal in water solutions at low solute concentrations,[59] and therefore, its use for estimation purposes is not suitable. On the one hand, to the best of our knowledge, there is no other correlation or approach that can be used to estimate the MS diffusion coefficient of CO_2 in brine.

However, the use of the Darken relation translates the problem of the estimate of the diffusion coefficient to the estimate of the self-diffusion coefficient. Experimentally, self-diffusion coefficient (D_i^{self}) and rotational relaxation times can be measured by Proton magnetic resonance (^{1}H-MR) for water and spin−lattice NMR for $^{13}CO_2$. However, we have not been able to find any data on these properties to straightforwardly make the estimate using the Darken relation and to compare to our simulation results. Hence, in this section we propose an alternative route using the information on the rotational relaxation times or the calculated self-diffusion coefficients (given in Tables B1−B9 of the Supporting Information) in order to predict D_{2b}^{MS} at different thermodynamic conditions.

To derive this correlation, first we recall that the rate of rotational relaxation is commonly explained by using the viscosity dependence and the orientational correlation time, τ_R,

dx.doi.org/10.1021/jp2081758 | J. Phys. Chem. B 2012, 116, 2787−2800

which is given by the well-known Debye−Stokes−Einstein (DSE) relation[60]

$$\tau_R = \frac{C_R \eta \nu_S}{k_B T} \tag{38}$$

where ν_s is the specific volume of the solute molecule; C_R is a constant equal to 3 in the DSE theory but left in general as a fitting constant; and η is the viscosity of the solvent. From eq 38 we can see that τ_R/η is a constant for a particular solute−solvent pair. It was suggested that the rotation of a probe molecule in a viscous liquid should be coupled to the structural relaxation of the surrounding solvent;[60] thus, in this sense, it is analogous to the self-diffusion. Starting form the Stokes−Einstein (SE) relation it is know that the translational diffusion of one solute molecule (D_i^{self}) may also be expressed in terms of solvent viscosity (η) and the radius of the molecule (R), according to

$$D_i = \frac{k_B T}{C_T \eta R} \tag{39}$$

Here, C_T is another constant. A direct relation can be then expressed between eqs 38 and 39, as follows

$$\tau_R D_i = \frac{C_R \nu_S}{C_T R} \tag{40}$$

which depend only on constants and geometric dimensions of the molecule. In ref 60 the author found a microscopic expression for the constants in eq 40 relating them to dynamic structure factors obtained from mode coupling theory. Notice that this equation does not depend on the solvent viscosity and that it can be generalized to different dissolved gas molecules with the only condition of low concentration (infinite dilution). We should mention, however, that such an approximation is only valid on relatively dense systems (liquids), where the relaxation dynamics of the dissolved molecule is governed by the friction with the surrounding medium. We thus use eq 40 to determine C_R and C_T for CO_2 dissolved in brine using our simulation results of $D_{CO_2}^{self}$ and $\tau_{C=O}$. The advantage of this procedure is that the self-diffusion coefficient of CO_2 shows less statistical fluctuation than the MS diffusion coefficient since the independent molecules all contribute to the statistics instead of only the baricenter (see Tables B1−B9 in the Supporting Information). We have also assumed that CO_2 has no rotational relaxation time other than $\tau_{C=O}$. Then, from the more precise evaluation of the self-diffusion coefficient as well as the rotational relaxation time, the unknown constants can be fitted, according to a linear function of the density

$$\tau_{C=O}^{l} D_{CO_2}^{self} \frac{R_{CO_2}}{\nu_{CO_2}} = \frac{C_R}{C_T} = (a_1(l) + a_2(l)\rho) \tag{41}$$

where l is the order of the associated Legendre polynomial (i.e., l = 1, 2); a_1 and a_2 are constants; and ρ is the system density (in g/cm^3). Here we have used the fact that the product $\tau_{C=O}^{l} D_{CO_2}^{self}$ depends only on the system density[61,62] and structural properties of the molecules, which of course remain constant. In the determination of the coefficients of eq 41 we have used $\nu_S = 29.1936 \times 10^{-30}$ m^3 and $R_{CO2} = 1.9101 \times 10^{-10}$ m, which are the molar volume and hydrodynamic radius of the EPM2 model of CO_2, respectively. Details of the fitting procedure of eq 41 and estimation of ν_S and R_{CO2} are available in the Supporting Information. To estimate D_{CO2} with eq 41, we need to express the variation of the rotational relaxation of CO_2 as a function of temperature and salt concentration (c in molal). This was done by an Arrhenius fitting of the $\tau_{C=O}$ data shown in Figure 9. We obtain for a salinity of 1 $m < c < 4$ m and $T < 453$ K

$$A(l, c) = a_3(l) \cdot c^{a_4(l)} \tag{42}$$

and

$$\Delta E(l, c) = a_5(l) \ln(c) + a_6(l) \tag{43}$$

Again, a_i (i = 3,4, ..., 6) are constants which depend on the associated Legendre polynomial. Parameters a_i are shown in Table 5.

Table 5. Coefficients a_i Obtained for Equations 41, 42, and 43

coefficient	l	value	units
a_1	1	18.444	dimensionless
	2	8.8153	dimensionless
a_2	1	−14.042	cm^3/g
	2	−6.9448	cm^3/g
a_3	1	0.0749	s^{-1}
	2	0.0365	s^{-1}
a_4	1	−0.1877	dimensionless
	2	−0.1284	dimensionless
a_5	1	1.061	kJ/mol
	2	0.804	kJ/mol
a_6	1	8.378	kJ/mol
	2	7.942	kJ.mol^{-1}

Equation 41, together with eqs 42 and 43, permit us to find an estimate of the self-diffusion coefficient of CO_2 in brine in terms of the rotational relaxation time and state variables. We have finally used the predictions of eq 41 for the self-diffusion coefficient into eq 37 and compared the results with the mutual diffusion coefficient of CO_2 in brine obtained from simulations using eq 9, at all temperatures and salt concentrations in Figure 10. We observe a general good agreement between the values

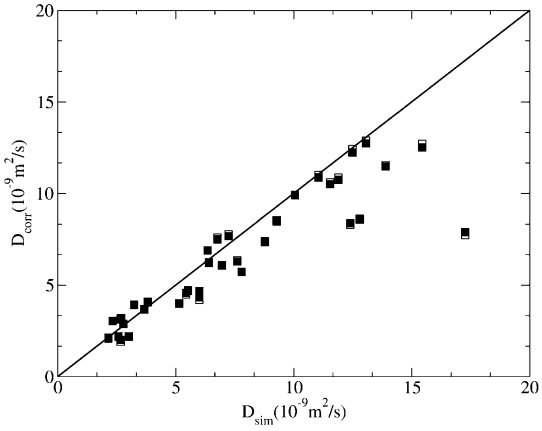

Figure 10. Comparison of the MS diffusion coefficient obtained with the correlation of eq 36 (with l = 1, full symbols, l = 2 empty symbols) with the simulation results for the MS diffusion coefficient using eq 9 ($D_{sim} = D_{2b}^{MS}$). The points that deviate more from the line $D_{sim} = D_{corr}$ are the simulations at high temperature and c = 4 m.

simulated and predicted, with an absolute average deviation of about 15.4% for the MS diffusion of CO_2. Recently Yeh et al.

dx.doi.org/10.1021/jp2081758 | J. Phys. Chem. B 2012, 116, 2787−2800

proposed a correlation to correct the results for the self-diffusion coefficient for the finite size effect unavoidable in common molecular dynamic simulations.[63] We did not correct our simulation results for this effect, however, since we have used a quite large number of particles (at least 3000 water molecules). We estimate that our reported values for self-diffusion may be underpredicted by a maximum of 6.5%. Therefore, the general good agreement of the correlation may suggest that the direct evaluation of the MS diffusion coefficients at high dilution strongly deviates from what is expected, in view of our previous analysis.

5. CONCLUSIONS

We have computed MS as well as Fick diffusion coefficients of CO_2 in brine at thermodynamic conditions representative of deep saline aquifers using MD simulations. To achieve this goal, Einstein and GK formulations have been used.

To test the accuracy of the chosen intermolecular potentials for the different species, validation tests were performed for NaCl−water and CO_2−water systems. For aqueous ionic solutions, WN Lennard-Jones parameters for ion−ion interactions were chosen as they reproduce better electrolytic solution densities for high salt concentrations than the Dang set of LJ parameters. Simulation results for MS diffusion coefficients of ions in water agree with experimental data (mean deviation ≈ 10%) and with WN simulation results. Simulated MS diffusivities of Na^+ in Cl^- did not have the correct trend with salt concentration. The calculated electrical conductivity of aqueous NaCl was also compared to experimental data. Although for low salt concentrations our results are in agreement with experiments, electrical conductivity is underpredicted for 4 *m* salt concentrations. Simulated MS diffusion coefficients of CO_2 in water were computed at $P = P_{atm}$ and $P > P_{atm}$. Results were compared with experiments and with values obtained using the Wilke−Chang correlation. For $P = P_{atm}$, simulation results at $T = 298.15$ K agree with experiments, while results at $T = 283.15$ K have a deviation of 25% from experiments. This observed deviation was due to the low number of CO_2 molecules present in the system (2 and 3, respectively). For $P > P_{atm}$ a mean deviation of 18% was obtained between our simulation results and Wilke−Chang correlation results. It was an expected result as the Wilke−Chang correlation gives the mutual diffusion coefficient at infinite dilution.

The next step was the calculation of the CO_2 MS diffusion coefficient in brine. The influence of temperature, CO_2 concentration, and salinity was analyzed. MS diffusivities increase with temperature. For all fixed pressures, no significant effect of CO_2 pressure was observed. The evaluated MS diffusion coefficients show a small but consistent dependence with the salinity. Electrical conductivity of CO_2−brine mixtures was also computed for all thermodynamic conditions using Einstein and GK formulations. As observed for MS diffusivities, the electrical conductivity increases with increasing temperature. In opposition to the observation for simulated MS diffusivities, electrical conductivities are clearly functions of salinity, increasing when the salt concentration increases. No CO_2 concentration dependence for electrical conductivity was clearly observed. Finally, simulated electrical conductivities at $T = 333.15$ K and $c = 1$ and 2 *m* were compared with values obtained using Fleury−Deschamps correlation. A shift is observed between simulation and correlation values.

MS diffusivity dependence with CO_2 concentration is a known difficult trend to determine not only by molecular simulation but also experimentally. We have proposed a correlation to estimate the diffusion coefficient based on the rotational relaxation time of CO_2 based on the variation of the product $\tau_{C=O}{}^{l} D_{CO_2}{}^{self}$ as a function of the system density. In this case, we were able to correlate our simulation results to predict the self-diffusion coefficient and MS diffusion coefficient with 15.4% of absolute deviation. However, both experimental and simulated Fick diffusion coefficients of even simple mixtures present large fluctuations with the quantity of CO_2 dissolved. In the literature, Zabala et al.[19] compared simulated Fick binary diffusion coefficients of CO_2 dissolved in nC10 as a function of x_{CO2} at saturation with experimental data.[64]

Finally, D_{2b}^{MS} decreases when increasing salt concentration likely due to the electrostatic interaction with the ions in solution.

■ ASSOCIATED CONTENT

Supporting Information

Details of the simulation data and other computational details are provided for the system studied. This material is available free of charge via the Internet at http://pubs.acs.org.

■ AUTHOR INFORMATION

Corresponding Author

*E-mail: carlos.nieto@ifpen.fr. Phone: 33-(0)1 47 52 58 60. Fax: 33-(0)1 47 52 70 58.

Notes

The authors declare no competing financial interest.

■ ACKNOWLEDGMENTS

We are indebted to the Ministerio de Ciencia e Innovación of the Spanish Government (J.B.A. and M.G.-R. acknowledge for grant CTQ2008-06469/PPQ). Finally, the authors thank the Programa d'ajuts de Recerca Cooperativa URV/ICIQ 2007 for financial support.

■ REFERENCES

(1) Core Writing Team; Pachauri, R. K.; Reisinger, A. *IPCC Fourth Assess-ment Report: Climate Change 2007: The AR4 Synthesis Report*; Cambridge University Press, 2007.
(2) Johansson, T. B.; Williams, R. H.; Ishitani, H.; Edmonds, J. A. *Energy Policy* **1996**, *24*, 985.
(3) Bachu, S.; Gunter, W. D.; Perkins, E. H. *Energy Convers. Manage.* **1994**, *35*, 269.
(4) Bachu, S. *Energy Convers. Manage.* **2000**, *41*, 953.
(5) Hitchon, B.; Gunter, W. D.; Gentzis, T.; Bailey, R. T. *Energy Convers. Manage.* **1999**, *40*, 825.
(6) Korbol, R.; Kaddour, A. *Energy Convers. Manage.* **1995**, *36*, 509.
(7) White, D. J.; Burrowes, G.; Davis, T.; Hajnal, Z.; Hirsche, K.; Hutcheon, I.; Majer, E.; Rostron, B.; Whittaker, S. *GSA Today* **2004**, *14*, 4−10.
(8) Information has been taken from: http://www.albertaasap.com/.
(9) Brosse, E. *Pétrole Tech.* **2001**, *435*, 50.
(10) Linstrom, P. J.; Mallard, W. G. *NIST Chemistry WebBook*, NIST Standard Reference Data Number 69; National Institute of Standards and Technology: Gaithersburg, MD, 2005.
(11) Li, Z.; Dong, M.; Li, S.; Dai, L. *J. Chem. Eng. Data* **2004**, *49*, 1026.
(12) Portier, S. Solubilité de CO_2 dans les saumures des bassins sédimentaires. *PhD Thesis*, Strasbourg, 2005; pp 1−257.
(13) Oeschger, H.; Siegenthaler, U.; Schotterer, U.; Gugelmann, A. *Tellus* **1975**, *27*, 168.

(14) Maier-Reimer, E.; Hasselmann, K. *Climate Dyn.* **1987**, *2*, 63.
(15) Lagneau, V.; Pipart, A.; Catalette, H. *Oil Gas Sci. Technol.-Rev. IFP.* **2005**, *60*, 231.
(16) Krishna, R.; Wesselingh, J. A. *Chem. Eng. Sci.* **1997**, *52*, 861−911.
(17) Krishna, R.; van Baten, J. M. *Ind. Eng. Chem. Res.* **2005**, *44*, 6939.
(18) Wheeler, D. R.; Newman, J. *J. Phys. Chem. B.* **2004**, *108*, 18353.
(19) Zabala, D.; Nieto-Draghi, C.; de Hemptinne, J.-C.; López de Ramos, A. *J. Phys. Chem. B.* **2008**, *112*, 16610.
(20) Kjelstup, S.; Bedeaux, D.; Johannessen, E.; Gross, J. *Non-equilibrium thermodynamics for engineers*; World Scientific: NJ, 2010.
(21) Taylor, R.; Krishna, R. *Multicomponent Mass Transfer*; John Wiley & Sons, Inc.: New York, 1993.
(22) Rothschild, W. G. *Dynamics of Molecular Liquids*; Wiley: New York, 1984. Berne, B. J.; Pecora, R. *Dynamic Light Scattering*; Wiley: New York, 1976. Fleming, R. *Chemical Applications of Ultrafast Spectroscopy*; Oxford University Press: New York, 1986.
(23) McConell, J. *The Theory of nuclear Magnetic Relaxation in Liquids*; Cambridge University: Cambridge, U.K., 1987.
(24) Holz, M.; Haselmeier, R.; Dyson, A. J.; Huber, H. *Phys. Chem. Chem. Phys.* **2000**, *2*, 1717.
(25) Umecky, T.; Kanakubo, M.; Ikushima, Y. *J. Phys. Chem. B* **2003**, *107*, 12003.
(26) Versmold, H. *Mol. Phys.* **1981**, *43*, 383.
(27) Kohlrausch, F. *Pogg. Ann.* **1863**, *119*, 337.
(28) Williams, G.; Watts, D. C. *Trans Faraday Soc.* **1970**, *66*, 80.
(29) Soreide, I.; Whitson, C. *Fluid Phase Equilib.* **1992**, *77*, 217.
(30) Berendsen, H. J. C.; Grigera, J. R.; Straatsma, T. P. *J. Phys. Chem.* **1987**, *91*, 6269.
(31) Pekka, M.; Lennart, N. *J. Phys. Chem. A* **2001**, *105*, 9954.
(32) Guardia, E.; Laria, D.; Marti, J. *J. Mol. Liq.* **2006**, *125*, 107114.
(33) Guardia, J.; Marti, J.; Padro, J. *Theor. Chem. Acc.* **2006**, *115*, 161169.
(34) Guardia, E.; Laria, D.; Marti, J. *J. Phys. Chem. B* **2006**, *110*, 6332.
(35) Guardia, E.; Marti, J.; GarciaTarres, L.; Laria, D. *J. Mol. Liq.* **2005**, *117*, 6367.
(36) Harris, J. G.; Yung, K. H. *J. Phys. Chem.* **1995**, *99*, 12021.
(37) Dang, L. X. *J. Am. Chem. Soc.* **1995**, *117*, 6954.
(38) Fincham, D. *Mol. Simul. B* **1992**, *8*, 165.
(39) Duan, Z.; Sun, R. *Chem. Geol.* **2003**, *193*, 257.
(40) Himmelblau, D. M. *Chem. Rev.* **1964**, *64*, 527.
(41) Saha, A. K.; Bandyopadhyay, S.; Biswas, A. K. *J. Chem. Eng. Data* **1993**, *38*, 78.
(42) Tamini, A.; Rinker, E. B.; Sandall, O. C. *J. Chem. Eng. Data* **1994**, *39*, 330.
(43) Versteeg, G. F.; Van Swaalj, W. P. M *J. Chem. Eng. Data* **1988**, *33*, 29.
(44) Wilke, C. R.; Chang, P. *Am. Inst. Chem. Eng. J.* **1955**, *1*, 264.
(45) Hayduk, W.; Laudie, H. *Am. Inst. Chem. Eng. J.* **1974**, *20*, 611.
(46) Tyn, M. T.; Calus, W. F. *Processing* **1975**, *21*, 16.
(47) Fleury, M.; Deschamps, H. *J. Chem. Eng. Data* **2008**, *53*, 2505.
(48) Chapman, T. W. The Transport Properties of Concentrated Electrolytic Solutions. *Ph. D. Thesis*, University of California, 1967.
(49) Davidson, J. F.; Cullen, M. A. *A. Trans. Inst. Chem. Eng.* **1957**, *35*, 51.
(50) *International Critical Tables*; McGraw-Hill Book Co.: New York, 1928; Vol. *3*, p 259.
(51) Diamond, L.; Akinfiev, N. *Fluid Phase Equilib.* **2003**, *208*, 265.
(52) Lisal, M.; Smith, W. R.; Aim, K. *Fluid Phase Equilib.* **2004**, *226*, 161.
(53) Marti, J.; Nagy, G.; Guardia, E.; Gordillo, M. C. *J. Phys. Chem. B.* **2006**, *110*, 23987.
(54) Glättli, A.; Daura, X.; Van Gunsteren, W. F. *J. Chem. Phys.* **2002**, *116*, 9811.
(55) Guardia, E.; Marti, J. *Phys. Rev. E.* **2004**, *69*, 11502.
(56) Guardia, E.; Laria, D.; Marti, J. *J. Phys. Chem. B* **2006**, *110*, 6332.
(57) Darken, L. S. *Trans. Am. Inst. Min. Metall. Eng.* **1948**, *175*, 184.
(58) Caldwell, C. S.; Babb, A. L. *J. Phys. Chem.* **1956**, *60*, 51.
(59) Taylor, R.; Krishna, R. In *Multicomponent Mass Transfer*; Wiley-Interscience, Har/Dskt ed.: New York, 1993.
(60) Bagchi, B *J. Chem. Phys.* **2001**, *115*, 2207.
(61) Ravichandran, S.; Bagchi, B. *J. Chem. Phys.* **1999**, *111*, 7505.
(62) Allen, M. P.; Camp, P. J.; Monson, C. P.; Evans, G. T.; Masters, A. J. *J. Chem. Phys.* **1996**, *105*, 11175.
(63) Yeh, I. C.; Hummer, G. *J. Phys. Chem. B* **2004**, *108*, 15873.
(64) Grogan, A. T.; Pinczewski, V. W.; Ruskauff, G.; Orr, F. M., Jr. *SPE Reservoir Engineering* (Paper SPE 14897), 1988; p 93.